arXiv:1402.5943v1 [cond-mat.quant-gas] 24 Feb 2014

Observation of geometric scaling of Efimov states in a Fermi-Bose Li-Cs mixture

Shih-Kuang Tung, Karina Jiménez-García, Jacob Johansen, Colin Parker, and Cheng Chin*
The James Franck Institute, The Enrico Fermi Institute, and Department of Physics, The University of Chicago, Chicago, Illinois 60637, USA

(Dated: February 25, 2014)

The emergence of scaling symmetry in physical phenomena suggests a universal description that is insensitive to microscopic details. A well known example is critical phenomena, which are invariant under continuous scale transformations and classify second-order phase transitions into distinct universality classes [1]. Equally intriguing are systems with discrete scaling symmetry, which are invariant under scaling transformation with a specific scaling constant, resulting in log-periodic behavior in the observables [2]. A classic example is the self-similar growth of crystals, as in snowflakes. In few-body physics, Vitaly Efimov predicted in 1970 the existence of an infinite series of three-body bound states that obey universal discrete scaling symmetry when pair-wise interactions are resonantly enhanced [3]. Despite abundant reports of Efimov states in cold atom experiments [4–13], direct observation of discrete scaling symmetry remains an elusive goal. Here we report the observation of three Efimov resonances in a heteronuclear Li-Cs mixture near a broad interspecies Feshbach resonance [14, 15]. The positions of the resonances provide a model-independent confirmation of discrete scaling symmetry with an averaged scaling constant $\lambda_{\rm exp} = 4.85(44)$, in good agreement with the predicted value of 4.88 [16, 17]. Our findings also provide new insight into the possible discrete scaling symmetry in Bose gasses and mixtures with resonant interactions.

In the Efimov scenario, while pairs of particles with short-range resonant interactions can not be bound, there exists an infinite series of three-particle bound states. Efimov states originate from an attractive $1/R^2$ effective potential in hyperspherical coordinates, where the hyperspherical radius R characterizes the size of the system. These bound states have universal properties insensitive to the short range details of the molecular potential and display discrete scaling symmetry; the size R_n and binding energy E_n of the n-th lowest Efimov state scale geometrically as $R_n = \lambda R_{n-1}$ and $E_n = \lambda^{-2} E_{n-1}$, where λ is the scaling constant. An alternative picture to understand discrete scaling symmetry was developed based on renormalization group limit cycles [18]. Away from the two-body scattering resonance, Efimov states couple to the scattering continuum and induce a series of three-body scattering resonances at scattering lengths $a = a_-^{(n)} < 0$, which also follow the scaling law $a_-^{(n)} = \lambda a_-^{(n-1)}$ [19] (see Fig. 1).

Ultracold atoms are an ideal system to test Efimov scaling symmetry given that their interatomic interactions can be tuned over several orders of magnitude using Feshbach resonances [20]. The emergence of Efimov states can be detected from the three-body recombination rate. The first evidence of an Efimov state was reported in ultracold Cs atoms near a Feshbach resonance [4]; subsequent observations of Efimov resonances in homonuclear systems were also reported in ^{7}Li [6, 7], ^{39}K [8], ^{85}Rb [12], ^{133}Cs [11], and ^{6}Li [5, 9]. Despite these numerous observations, the experimental confirmation of the discrete scaling symmetry remains a challenging goal.

Universal discrete scaling symmetry is the most remarkable feature of Efimov states and its confirmation requires the observation of multiple Efimov resonances. With two consecutive Efimov resonances, the scaling symmetry can be tested through a comparison between the ratio of the resonance positions and the theory; in contrast, with three or more resonances one can perform a model independent test. The observation of multiple resonances is challenging experimentally because the signature of higher order Efimov resonances diminishes when the scattering rate is unitarity limited [4, 21, 22]. This challenge is acute in homonuclear systems, where the scaling constant is $\lambda \approx 22.7$ [3] and the detection of an additional Efimov state demands a reduction of temperature by a factor of $\lambda^2 \approx 515$.

Systems of different particles (heteronuclear systems) display Efimov scaling symmetry with a scaling constant λ, determined by the relative masses of the particles, quantum statistics, and which of the particles interact resonantly. A favorable system consists of one light atom resonantly interacting with two heavy atoms with a large mass ratio, for which the scaling constant can be significantly lower than 22.7 [16–18, 23]. On the other hand, experiments in heteronuclear systems are considerably more challenging than those in homonuclear systems. Observations of Efimov resonances in heteronuclear systems are scarce and have only been reported in K-Rb mixtures. A single Efimov resonance associated with each of the ^{41}K^{87}Rb^{87}Rb and ^{41}K^{41}K^{87}Rb trimers was observed at the three-atom scattering continuum [10]. In a later experiment using ^{40}K and ^{87}Rb, no Efimov resonances were observed at the three-atom scattering continuum, and an Efimov-like resonance between ^{40}K^{87}Rb molecules and ^{87}Rb atoms was identified at the atom-molecule scattering continuum [13].

Here we report the observation of discrete scaling symmetry of Efimov states in a Fermi-Bose mixture of ^{6}Li and ^{133}Cs. Taking advantage of the large mass ratio be-

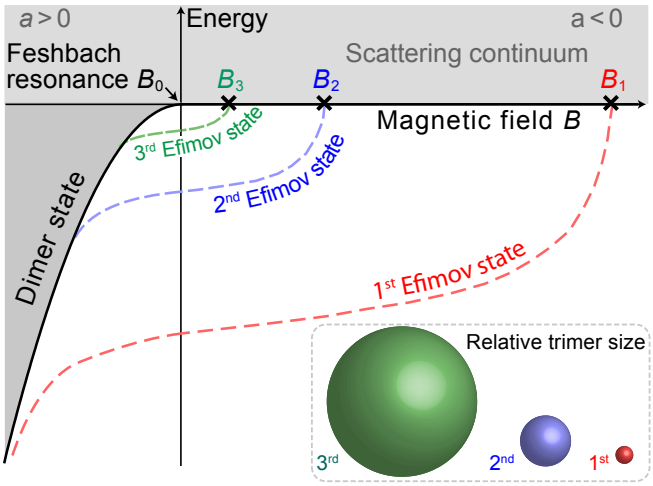

FIG. 1. **Discrete scaling symmetry of Efimov states.** A series of Efimov states (dashed curves) exists near a Feshbach resonance located at B_0. Away from the resonance, on the side with scattering length $a < 0$, they emerge at the three-body scattering continuum (crosses) causing an enhanced three-body recombination rate. Physical observables in the Efimov scenario are predicted to show discrete scaling symmetry; these include the size R_n, the binding energies E_n, and the location of the Efimov resonances at the scattering length a_n (associated with the magnetic field B_n). The discrete scaling law, followed by the location of the Efimov states and their relative molecular size, is graphically represented by the location of the resonances on the B-axis and the size of the spheres, respectively.

tween Li and Cs atoms, with a predicted scaling constant $\lambda = 4.88$ [16, 17], we identified three consecutive Efimov resonances near a wide, isolated s-wave interspecies Feshbach resonance [14]. Based on the measured locations of the resonances we determine a scaling constant $\lambda_{\rm exp} = 4.85(44)$.

Our experiment is based on a mixture of ^{6}Li and ^{133}Cs atoms near quantum degeneracy in an optical dipole trap. We prepare mixtures with up to $N_{\rm Li} = 3.4\times10^4$ Li atoms, and $N_{\rm Cs} = 5.2 \times 10^4$ Cs atoms at temperatures in the range 190 nK $< T <$ 800 nK. At even lower temperatures the two atomic species no longer overlap (Supplementary Information). We sequentially load Li and Cs atoms into two independent, spatially separated dipole traps and adiabatically merge them in a single trap. We polarize Li and Cs in their lowest hyperfine states to prevent two-body collisional loss. Following the merge process, we compress the trap to maximize the spatial overlap of the two species and prepare the sample at an initial magnetic field of 890 G, where the mixture is stable at a small interspecies scattering length $a_{\rm LiCs} = -22\ a_0$ and a_0 being the Bohr radius. Then the magnetic field is ramped in ~ 1 ms to a variable value B near the Feshbach resonance at B_0, giving a variable scattering length $a_{\rm LiCs}$.

Efimov resonances manifest, in our experiment, as enhanced atom loss due to three-body recombination collisions in which three colliding atoms resonantly couple to an Efimov state and then decay into a deeply bound molecule and a free atom. The released binding energy of the diatomic molecule is converted into kinetic energy and distributed between the molecule and the free atom, allowing them to escape the trap. We measure the Li and Cs atom numbers, from which we infer atom loss and identify the Efimov resonances. We present measurements of atom loss both as a function of hold time t, and as a function of magnetic field B. In addition, we extract the temperature using the time of flight technique.

The mixture of ^{6}Li and ^{133}Cs has two primary inelastic collision pathways based on the three-body recombination processes Cs-Cs-Cs and Li-Cs-Cs. Li-Li-Cs as well as Li-Li-Li collisions are strongly suppressed by Fermi statistics at low temperatures. This work focuses on the search for Efimov resonances associated with LiCsCs Efimov bound states near the broad Li-Cs Feshbach resonance located near 843 G [14]. The reported Efimov resonances are away from the p-wave Feshbach resonances observed in a Li-Cs mixture [15], as well as the known Cs Feshbach and Efimov resonances [11, 24].

Around the magnetic field region probed in this work, the magnitude of the Cs-Cs scattering length is large ($-2500a_0 \le a_{\rm CsCs} \le -1000a_0$) and three-body recombination of Cs atoms is the major competing loss process, imposing a limitation on the lifetime of Cs. Since $a_{\rm CsCs} < 0$, we do not expect the formation of Cs Feshbach molecules through recombination, and the analysis of the number loss data is simplified. Away from the Li-Cs Feshbach resonance Cs decay is dominated by Cs-Cs-Cs recombination collisions (Fig. 2a); on the other hand, Li decays much faster in the presence of Cs, indicating the dominance of interspecies collisional loss. Near the Feshbach resonance (Fig. 2b) both the decays of Li and Cs are significantly enhanced by interspecies collisions.

Our measurements of atom loss and the observation of Efimov resonances are summarized in Figure 3. In order to obtain the necessary statistics to precisely identify the Efimov resonances, we averaged several hundred data sets. To eliminate the long term drift in atom number, we scale the atom number so that it averages to unity over a fixed magnetic field range. Each panel shows loss features in the scaled number: the strongest feature comes from an interspecies Feshbach resonance (vertical dashed lines), with additional features arising from Efimov resonances (arrows). Interspecies loss features are suppressed in Cs due to strong Cs-Cs-Cs recombination.

Based on empirical fits (Supplementary Information), we determine the Feshbach and Efimov resonance positions to be $B_0 = 842.75(1)$ G, $B_1 = 848.36(16)$ G, $B_2 = 843.82(2)$ G, and $B_3 = 842.97(4)$ G. In addition to these statistical uncertainties, there is a systematic magnetic field calibration uncertainty of 30 mG. The location

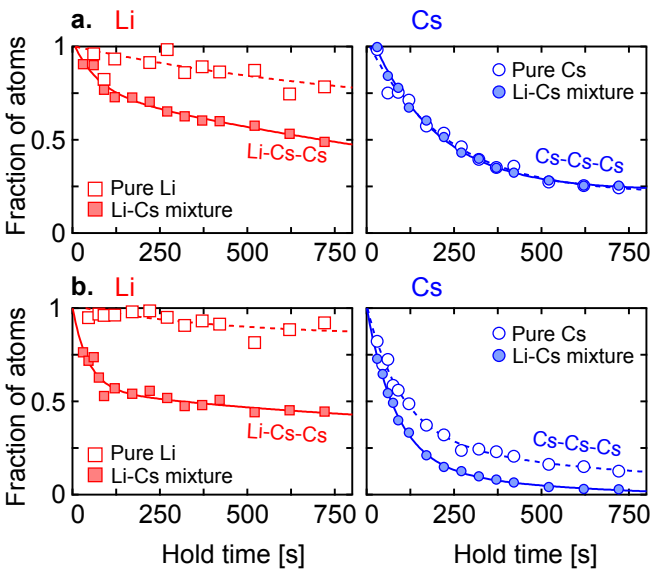

FIG. 2. **Atom number decay of single-species and Li-Cs mixture samples. a.** Atom fraction versus time at B =848.0 G, 5 G away from the Li-Cs Feshbach resonance ($a_{\mathrm{LiCs}} = -370\ a_0$, $a_{\mathrm{CsCs}} = -1240\ a_0$). Sample temperature is $T = 390$ nK. Li loss increases significantly when Cs is introduced (left panel). Cs loss is dominated by Cs-Cs-Cs recombination (right panel). The data are scaled to the initial atom numbers $N_{\mathrm{Li}} = 2.1 \times 10^4$ and $N_{\mathrm{Cs}} = 5.1 \times 10^4$ determined from empirical fits (Supplementary Information). **b.** Atom fraction versus time near the Li-Cs Feshbach resonance $B = 842.7$ G ($a_{\mathrm{CsCs}} = -2500\ a_0$), where enhanced atom loss is evident in both the Li and Cs atom number evolution when both species are present. The data are scaled to the initial atom numbers $N_{\mathrm{Li}} = 3.2 \times 10^4$ and $N_{\mathrm{Cs}} = 4.5 \times 10^4$. Sample temperature is $T = 340$ nK. Single species (mixture) data are shown by open (solid) symbols.

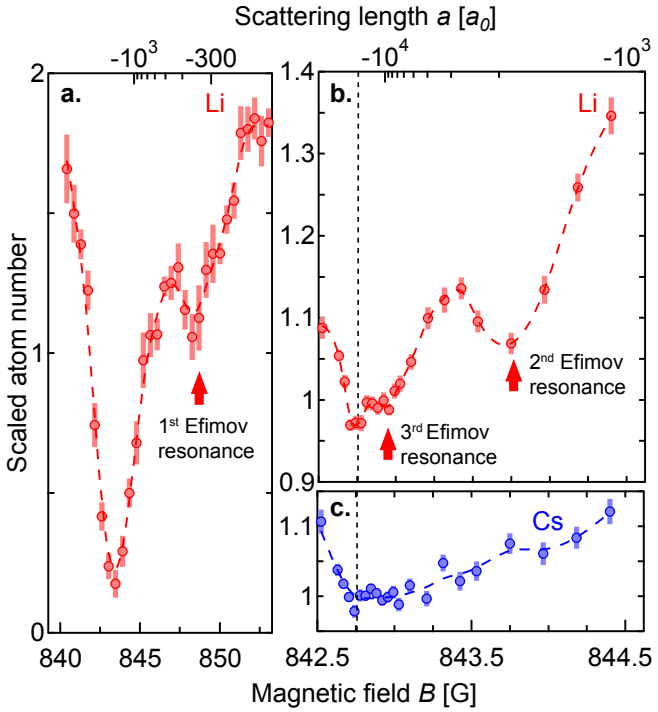

FIG. 3. **Observation of three Li-Cs-Cs Efimov resonances. a.** Scaled Li number versus magnetic field showing the first Li-Cs-Cs Efimov resonance. The mean atom numbers were $N_{\mathrm{Li}} = 1.3 \times 10^4$ and $N_{\mathrm{Cs}} = 2.7 \times 10^4$ with temperature $T = 800$ nK. **b-c.** Scaled Li (**b**) and Cs (**c**) numbers versus magnetic field showing the second and third Li-Cs-Cs Efimov resonances. The mean atom numbers were $N_{\mathrm{Li}} = 1.4 \times 10^4$ and $N_{\mathrm{Cs}} = 2.1 \times 10^4$ with temperature $T = 360$ nK. From empirical fits, the resonances are located 5.61(16), 1.07(3) and 0.22(4) G away from the Feshbach resonance (Supplementary Information). Due to finite temperature effects, the contrast of the third Efimov resonance is just a few percent. The scaled atom numbers come from the average of 13 (**a**) and 68 (**b**) individual traces normalized to their respective means. Typical hold times were 225 ms and 115 ms, respectively. The vertical dashed lines indicate the Feshbach resonance and arrows indicate the Efimov resonances. The dashed curves correspond to an interpolation of the the data and serve as guides to the eye.

of the Feshbach resonance deviates from our previous result obtained at a much higher temperature [14], where the Efimov structure was not resolved.

The relative positions of the Efimov resonances with respect to the Feshbach resonance $\Delta B_n = B_n - B_0$ are $\Delta B_1 = 5.61(16)$ G, $\Delta B_2 = 1.07(2)$ G and $\Delta B_3 = 0.22(4)$ G; these values provide a qualitative and direct evidence of the discrete scaling symmetry in this system with scaling $\Delta B_3 : \Delta B_2 : \Delta B_1 \approx 1 : 5 : 5^2$. Based on the revised value for B_0 and the width $\Delta = 62$ G of the interspecies Feshbach resonance [14], the observed Efimov resonances occur at the scattering lengths $a_-^{(1)} = -337(9)\ a_0$, $a_-^{(2)} = -1650(30)\ a_0$ and $a_-^{(3)} = -7900(1400)\ a_0$. We can form two scaling constants from the location of the three resonances: $\lambda_{21} = a_-^{(2)}/a_-^{(1)} = 4.90(16)$ and $\lambda_{32} = a_-^{(3)}/a_-^{(2)} = 4.79(87)$, which agree with each other within uncertainty. The averaged scaling constant is $\lambda_{\mathrm{exp}} = 4.85(44)$, and is in good agreement with the predicted value $\lambda = 4.88$ for Efimov states with resonant Li-Cs interactions [16, 17].

A number of effects can contribute to the small deviations between the observed scaling ratios and the predicted values. The first Efimov resonance can be shifted by finite-range corrections given that it occurs at a scattering length near the van der Waals length of Cs-Cs ($r_{\mathrm{CsCs}} = 101\ a_0$) and Li-Cs ($r_{\mathrm{LiCs}} = 45\ a_0$). (The ratio of $a_-^{(1)}$ to van der Waals length of the heavy particles, which is $-3.3(1)$ in our system, is expected to be universal for the light-heavy-heavy systems [17].) The location of Efimov resonances can also be shifted by finite temperature effects, which are stronger for resonances occurring at larger scattering lengths [26, 27]. We investigate the temperature dependence of the third Efimov resonance, as shown in Fig. 4, by performing multiple magnetic field

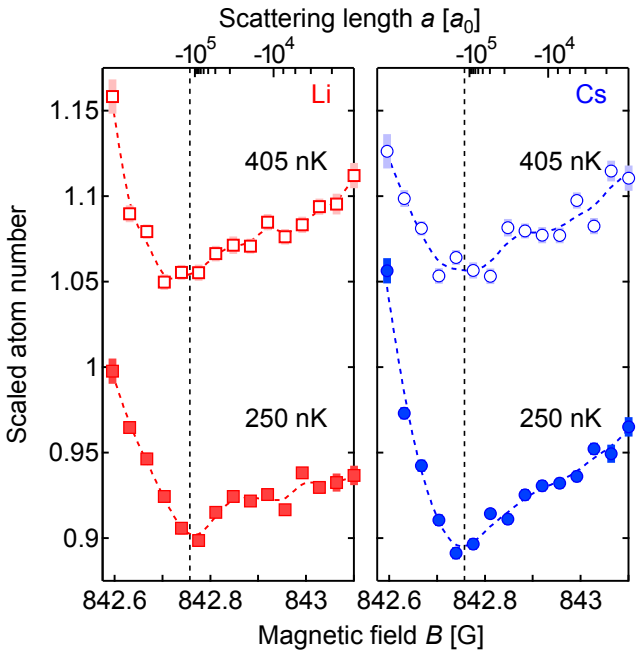

FIG. 4. **Location of the third Efimov resonance at different temperatures**. Scaled Li (squares) and Cs (circles) numbers versus magnetic field at mean temperature $T = 405$ nK (top) and mean temperature $T = 250$ nK (bottom). The mean atom numbers are $N_{\rm Li} = 1.4 \times 10^4$ and $N_{\rm Cs} = 1.3{\times}10^4$ (top), and $N_{\rm Li} = 1.3{\times}10^4$ and $N_{\rm Cs} = 7.0{\times}10^3$ (bottom). The scaled atom numbers come from the average of 209 (top) and 328 (bottom) individual traces normalized to their respective means. The typical hold time was 115 ms. Our measurements suggest that the location of the third Efimov resonance $B_3 = 842.97(4)$ G is not significantly shifted with temperature within our experimental resolution. The vertical dashed lines indicate the Feshbach resonance. The traces are offset vertically by 0.15 for clarity, and their interpolation (dashed curves) serves as guide to the eye.

scans with temperatures $T = 190-500$ nK. Due to a limited signal to noise ratio, we separate the data into two temperature groups with mean temperatures $T = 250$ nK and $T = 405$ nK. We average the scaled number from each group and do not observe significant temperature dependence in the resonance locations within our uncertainty. Our result is consistent with the theoretical calculations, which suggest a small thermal shift of less than 3% in the range of 100-1000 nK (Supplementary Information) [25]. Finally, the finite and slowly varying Cs-Cs scattering length in the magnetic field range we explore can lead to small systematic deviations of the measured scaling factors [17, 18].

In conclusion, we observe three Efimov resonances in a Li-Cs mixture and extract two scaling constants. From their mutual agreement and that with the theoretical calculation, we provide experimental evidence of geometric scaling symmetry of Efimov states. Based on our observation, an intriguing question is whether the discrete scaling symmetry can be seen in the original Efimov scenario of three identical bosons. In addition, our result hints at the discrete scaling symmetry in a unitary Bose gas, contrasting the continuous scaling symmetry in a unitary Fermi gas [28].

We acknowledge support from the NSF-MRSEC program, NSF Award No. PHY-1206095, and AFOSR-MURI. We wish to thank Yujun Wang for valuable conversations and for sharing his preliminary calculations, as well as Paul Julienne and Chris Greene for useful discussions.

Note: We have been recently become aware of the observation of the second Efimov state in a pure Cs sample [29].

* cchin@uchicago.edu

[1] H. Stanley, *Introduction to Phase Transitions and Critical Phenomena* (Oxford University Press, 1987).
[2] D. Sornett, Physics Reports **297**, 239 (1998).
[3] V. Efimov, Phys. Lett. B **33**, 563 (1970).
[4] T. Kraemer, M. Mark, P. Waldburger, J. G. Danzl, C. Chin, B. Engeser, A. D. Lange, K. Pilch, A. Jaakkola, H.-C. Nägerl, and R. Grimm, Nature **440**, 315 (2006).
[5] T. B. Ottenstein, T. Lompe, M. Kohnen, A. N. Wenz, and S. Jochim, Phys. Rev. Lett. **101**, 203202 (2008).
[6] S. E. Pollack, D. Dries, and R. G. Hulet, Science **326**, 1683 (2009).
[7] N. Gross, Z. Shotan, S. Kokkelmans, and L. Khaykovich, Phys. Rev. Lett. **103**, 163202 (2009).
[8] M. Zaccanti, B. Deissler, C. D'Errico, M. Fattori, M. Jona-Lasinio, S. Muller, G. Roati, M. Inguscio, and G. Modugno, Nature Phys. **5**, 586 (2009).
[9] J. H. Huckans, J. R. Williams, E. L. Hazlett, R. W. Stites, and K. M. O'Hara, Phys. Rev. Lett. **102**, 165302 (2009).
[10] G. Barontini, C. Weber, F. Rabatti, J. Catani, G. Thalhammer, M. Inguscio, and F. Minardi, Phys. Rev. Lett. **103**, 043201 (2009).
[11] M. Berninger, A. Zenesini, B. Huang, W. Harm, H.-C. Nägerl, F. Ferlaino, R. Grimm, P. S. Julienne, and J. M. Hutson, Phys. Rev. Lett. **107**, 120401 (2011).
[12] R. J. Wild, P. Makotyn, J. M. Pino, E. A. Cornell, and D. S. Jin, Phys. Rev. Lett. **108**, 145305 (2012).
[13] R. S. Bloom, M.-G. Hu, T. D. Cumby, and D. S. Jin, Phys. Rev. Lett. **111**, 105301 (2013).
[14] S.-K. Tung, C. Parker, J. Johansen, C. Chin, Y. Wang, and P. S. Julienne, Phys. Rev. A **87**, 010702 (2013).
[15] M. Repp, R. Pires, J. Ulmanis, R. Heck, E. D. Kuhnle, M. Weidemüller, and E. Tiemann, Phys. Rev. A **87**, 010701 (2013).
[16] J. P. D'Incao and B. D. Esry, Phys. Rev. A **73**, 030703 (2006).
[17] Y. Wang, J. Wang, J. P. D'Incao, and C. H. Greene, Phys. Rev. Lett. **109**, 243201 (2012).
[18] E. Braaten and H.-W. Hammer, Physics Reports **428**, 259 (2006).
[19] B. D. Esry, C. H. Greene, and J. P. Burke, Phys. Rev. Lett. **83**, 1751 (1999).
[20] C. Chin, R. Grimm, P. Julienne, and E. Tiesinga, Rev.

Mod. Phys. **82**, 1225 (2010).
[21] B. S. Rem, A. T. Grier, I. Ferrier-Barbut, U. Eismann, T. Langen, N. Navon, L. Khaykovich, F. Werner, D. S. Petrov, F. Chevy, and C. Salomon, Phys. Rev. Lett. **110**, 163202 (2013).
[22] R. J. Fletcher, A. L. Gaunt, N. Navon, R. P. Smith, and Z. Hadzibabic, Phys. Rev. Lett. **111**, 125303 (2013).
[23] K. Helfrich, H.-W. Hammer, and D. S. Petrov, Phys. Rev. A **81**, 042715 (2010).
[24] M. Berninger, A. Zenesini, B. Huang, W. Harm, H.-C. Nägerl, F. Ferlaino, R. Grimm, P. S. Julienne, and J. M. Hutson, Phys. Rev. A **87**, 032517 (2013).
[25] Y. Wang, Private communication.
[26] J. P. D'Incao, H. Suno, and B. D. Esry, Phys. Rev. Lett. **93**, 123201 (2004).
[27] H.-C. Närgerl, T. Kraemer, M. Mark, P. Waldburger, J. G. Danzl, B. Engeser, A. D. Lange, K. Pilch, A. Jaakkola, C. Chin, and R. Grimm, AIP Conference Proceedings **869**, 269 (2006).
[28] T.-L. Ho, Phys. Rev. Lett. **92**, 090402 (2004).
[29] R. Grimm, Private communication.

SUPPLEMENTAL MATERIAL

Magnetic field calibration

We use microwaves to drive Cs atoms from the lowest to the highest hyperfine state of the 6 $^2S_{1/2}$ manifold. We convert the observed transition frequency (typically 11315.3 MHz) into a magnetic field value using the Breit-Rabi formula. The average width of the spectroscopic signals is 30 kHz, corresponding to 12 mG in magnetic field. We observe drifts in the magnetic field of up to $\pm$40 mG, which we correct by regular calibration.

Atom number determination

After each experimental cycle, we perform absorption imaging on both atomic species. Li images are taken *in situ* at a magnetic field of 853 G, while Cs images are recorded after a 15 ms time of flight (TOF) near zero magnetic field, from which we measure its atom number and temperature.

Fitting the atom number evolution

Fitting the atom number evolution in a Li-Cs mixture suffers from multiple experimental complications, which prevent us from extracting the Li-Cs-Cs recombination coefficient without very large systematic uncertainties. First of all, the Li and Cs atomic clouds only partially overlap because of the great differences in their trapping potentials, masses, magnetic moments, and gravitational sags in the trap. In particular, the large difference in their gravitational sags of 16 μm also prevents us from experimenting with temperatures well 200 nK, for which the Li and Cs clouds completely separate. Secondly, Cs-Cs-Cs recombination plays a crucial role in the evolution of the Cs number, and, paritally, in Li number. This process requires a separate fitting model. Finally, near the Li-Cs Feshbach resonance and Li-Cs-Cs Efimov resonances, fast collision losses drive the sample far from thermal equilibrium, which not only influences the overlap of the clouds, but also introduce temperature dependence to the recombination rate. These effects together strongly limit our capability to extract the three-body recombination coefficient. Imperfect knowledge of the cloud overlaps and the non-equilibrium dynamics in the trap, in particular, introduce systematic uncertainties much greater than our statistical uncertainties and the precision required to identify Efimov resonances.

Shown in Figure 2, we instead adopt empirical fits to the atom number evolution $N(t) = N_0 + N_1 \exp(-t/\tau_1) + N_2 \exp(-t/\tau_2)$ for both Li an Cs atom numbers, where N_0 is the background atom number, and $\tau_1 < \tau_2$ characterizes the decay time constant at shorter times, τ_2 the time constant at longer times, and $N_{1,2}$ are the contributions from each term. To compare decays in pure and mixed samples, the atom numbers are scaled by the initial value $N(0) = N_0 + N_1 + N_2$.

Determination of Feshbach and Efimov resonance positions

The Li number is obtained by integrating *in situ* absorption images of Li atoms, while the Cs number and temperature are obtained from time-of-flight images. Atom numbers are recorded with magnetic field values. In order to obtain the necessary statistics to precisely identify the Efimov resonances, we need to average data taken over several days. As a result, even very minor long term drifts in experimental parameters had significant effects on atom number. To remove these drifts, we rescale our data so that it averages to one over a fixed magnetic field range. In addition, small changes in the magnetic field calibration require us to interpolate our data to a fixed set of fields. After rescaling and interpolating, we remove the top and bottom 10% of values at each magnetic field and average our data. Finally, we fit the positions of the Efimov resonances using a linear background with a Gaussian, $c_0 + c_1 B - c_2 \exp[-(B-c_3)^2/2c_4^2]$, where c_i are the fitting parameters (continuous curves in Fig. S1). The fits also determine the width of the resonance, from which we derive $\eta = 0.08(3)$ for the first Efimov resonance. The widths of the second and third Efimov states appear much broader due to finite temperature effects, see discussion below. Finally, we determine the position of the Feshbach resonance by fitting the associated loss feature to a parabola (dashed curve

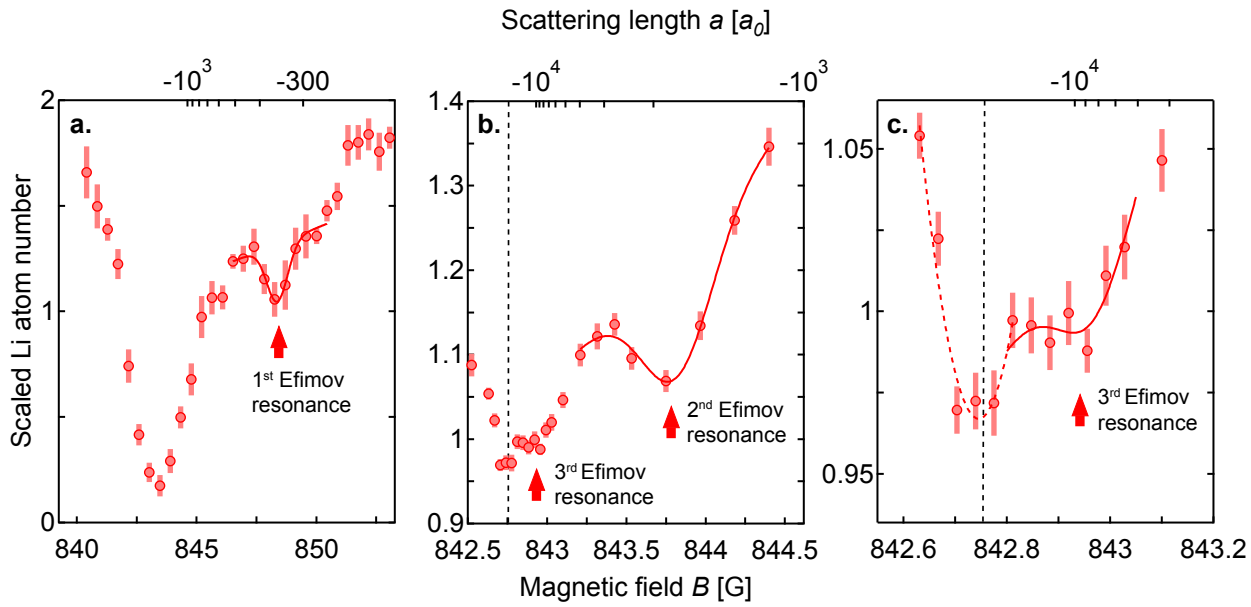

FIG. S1. **Empirical fits identifying the location of Feshbach and Efimov resonances.** Scaled Li atom number as a function of magnetic field. The location of Efimov resonances are determined from a superposition of linear and gaussian fits (continuous curves). The location of the Feshbach resonance (represented by vertical dashed lines) is determined by a quadratic fit to the data with largest resolution (dashed curve in **c**).

in Fig. S1c). The apparent Feshbach minimum in the coarse scan (Fig. S1a) is a convolution of the Feshbach resonance and the second and third Efimov resonances, and cannot reliably be used to determine the location of the Feshbach resonance.

Experimental Setup

Our experimental apparatus relies on a dual magneto-optical trap (MOT) and dynamic optical dipole traps to produce an ultracold mixture of ^{6}Li and ^{133}Cs. Laser cooled Li and Cs atoms are initially spatially separated in two independent optical dipole traps (denoted here as A and B) to avoid light-assisted collisional loss. The traps are later dynamically combined to achieve optimum trap loading and evaporation of both species.

Trap A is primarily used to confine Li atoms in the initial stage of the experiment and is generated by a pair of 1070 nm laser beams generated from a 200 W Yb fiber laser. The beams propagate parallel to the x-axis and are focused by a final lens. The beams cross at an angle $\theta = 15^\circ$ at the focus with $1/e^2$ radii of 40 μm. After loading Li atoms, trap A is spatially displaced up to 25 mm along the x-axis by moving the focusing lens [14]. This step is essential to avoid light-assisted collisional loss between Li and Cs atoms.

Trap B initially captures laser-cooled Cs atoms, and eventually confines both atomic species. The trap is formed at the intersection of two orthogonally propagating 1064 nm laser beams, whose intensities are independently controlled. The beam propagating along the z-axis has a $1/e^2$ radius of 400 μm, while the beam propagating along the x-axis has an elliptical cross section with $1/e^2$ radii of $w_z = 200$ μm and $w_y = 60$ μm. The elliptical beam is spatially modulated at 1.2 MHz along the y-axis (gravity direction) to dynamically increase the vertical size of trap B by about a factor of 3.

Dipole Trap Merging and Evaporation

Following the loading and evaporation of Li in trap A, we displace trap A and begin the loading and optical cooling of Cs. After a series of Raman sideband cooling stages Cs atoms are loaded into trap B. We denote the time following the last sideband cooling stage as $t_1 = 0$ ms. At this point the modulation of the elliptical beam is maximum (Fig. S2a) and a magnetic field gradient is applied to levitate only the lowest hyperfine state of Cs, giving us a high Cs spin purity. Subsequently we compress Cs atoms by reducing the modulation of the elliptical beam and increasing the intensity of Trap B. Simultaneously we ramp the magnetic field gradient to zero, until a tight optical trap is achieved at $t_2 = 2515$ ms. The tighter trap improves evaporation efficiency, and does not require magnetic levitation. This allows us to relax the Li in trap A from t_2 to $t_3 = 3705$ ms. At t_3 we also jump the magnetic field over 25 ms to 890 G where Cs evaporation can be most efficient. From t_3 to $t_4 = 10754$ ms we evap-

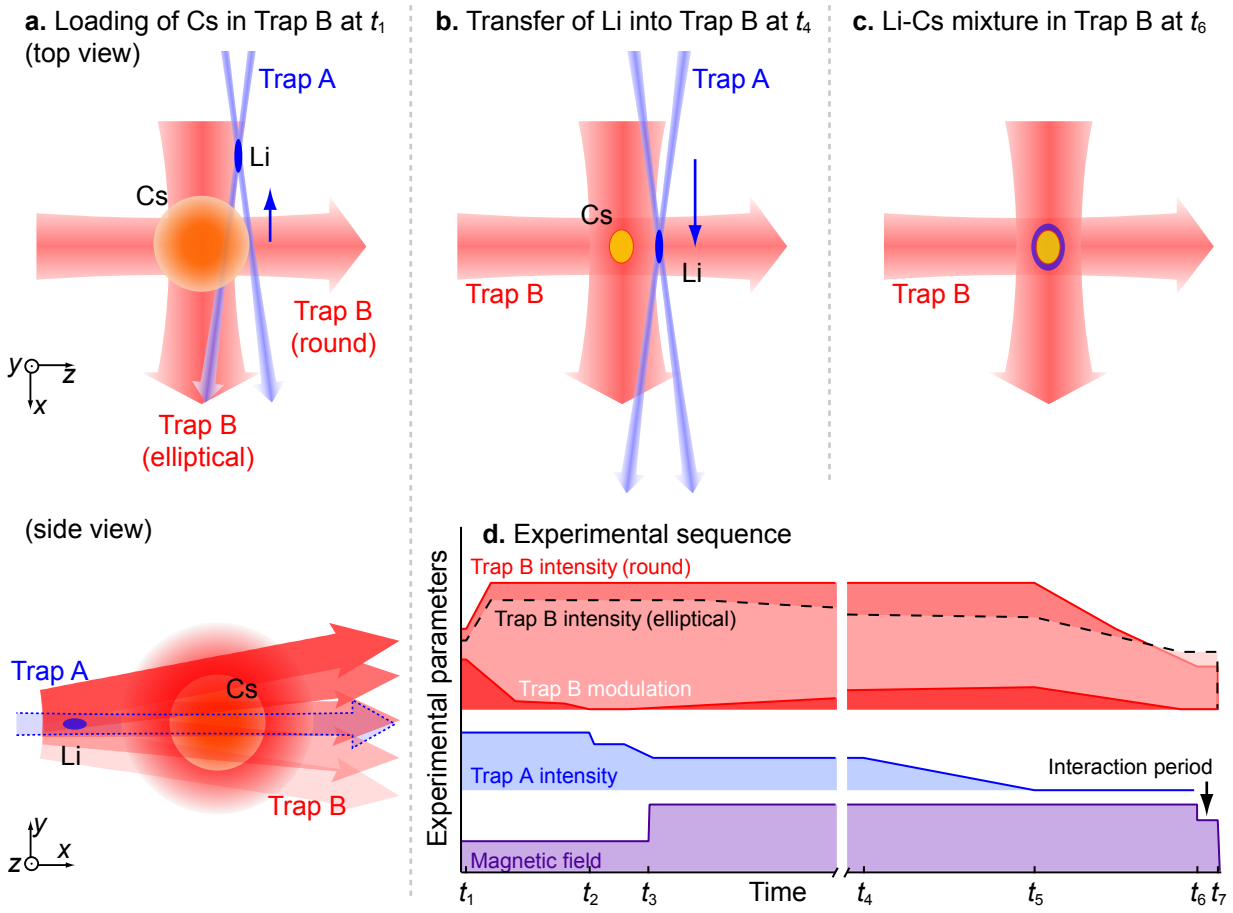

FIG. S2. **Schematic of our Li-Cs merge procedure**. The experimental sequence and the meaning of the time points t_i are described in the text. **a.** Schematic of Cs loading in trap B at maximum modulation (side view) while trap A is displaced along x. **b.** Location of trap A prior to the transfer after Li atoms from trap A to trap B. **c.** Schematic of the combined mixture in trap B. **d.** Experimental sequence.

orate Cs by increasing the modulation of the elliptical beam and decreasing its intensity. During this time we move trap A into the round beam of trap B (Fig. S2b). From t_4 to $t_5 = 11802$ ms we release the Li atoms from trap A into trap B by ramping the intensity of trap A to zero (Fig. S2c). The relative position of the traps before the release of Li atoms is offset vertically by ~ 100 μm and horizontally by ~ 200 μm; these coordinates are optimized experimentally to achieve suitable conditions for the atom-number loss measurements. If trap A is positioned too close to trap B, Cs atoms will leak and cause severe Li loss. On the other hand, if trap A is too far from trap B, the Li transfer efficiency into trap B will be low. Between t_5 and $t_6 = 12711$ ms, trap B intensity is decreased while the modulation is ramped to 0 so as to evaporate and compress into a trap where Li and Cs overlap. We also fire a short burst of light resonant with the second-to-lowest Li hyperfine state to remove these unwanted atoms while preserving the Li atoms in the lowest hyperfine state. At t_6, the magnetic field is jumped to a variable value, and finally the atoms are imaged at $t_7 = 12801$ ms. During the interaction period there is a minimum trap depth at which the species can be made to overlap, limiting Cs temperature to about 200 nK. The relevant experimental parameters are depicted in Fig. S2d.

Temperature dependence of Li-Cs Efimov resonances

Signatures of higher order Efimov resonances suffer from finite temperature effects when the thermal de Broglie wavelength $\lambda_{\rm dB}$ of the atoms is small compared to the scattering length at which the resonance occurs $a_-^{(n)}$. At the lowest temperature reported here (190 nK) we have $\lambda_{\rm dB} = 6500\ a_0$ for Cs and $\lambda_{\rm dB} = 30700\ a_0$ for Li, which are both much larger than the second Efimov resonance position $|a_-^{(2)}| = 1650\ a_0$, but comparable with the third resonance $|a_-^{(3)}| = 7900\ a_0$. This is consistent with our capability to see only three resonances. A temperature below 10 nK is needed to see the fourth resonance

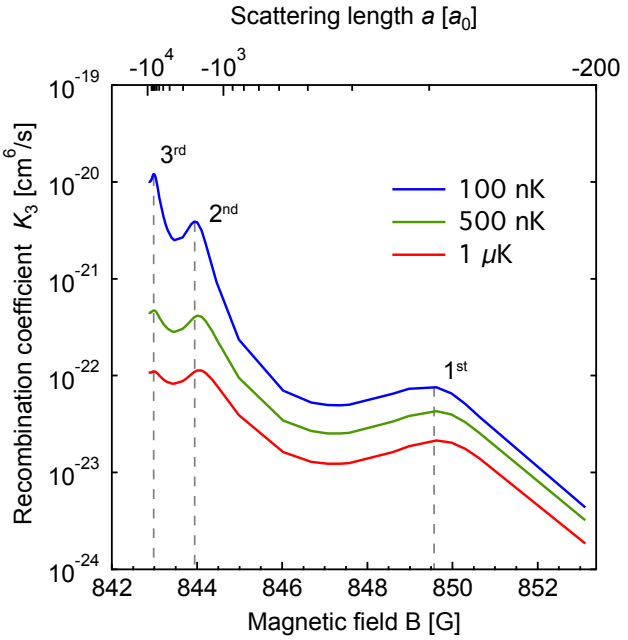

FIG. S3. **Theoretical calculation of the Li-Cs-Cs three-body recombination coefficient**. The calculation, conducted by Y. Wang [25], is based on the interaction parameters given in Ref. [14]. The enhancements of the recombination coefficient indicate Efimov resonance positions (dashed lines) and correspond to the dips in the scaled atom number shown in experiment (Fig. 3). At higher temperatures, weaker resonance features and small shifts of the resonance positions are evident.

in our system, which is currently beyond our reach.

In our system, the signatures of the Efimov resonance suffer from two finite temperature effects. Firstly, the contrast of the resonance features decreases from 25% for the first resonance to a few percent for the third one, see Fig. S1. Thus more averaging is required to identify the excited Efimov states. The apparent widths of the excited states also appear larger, leading to larger uncertainties in the determination of the decay parameter η. Secondly, finite temperature can lead to a shift of the resonance position, which we investigate and show in Fig. 4. Complementary to our experiment, an independent three-body calculation conducted by Y. Wang based on the scattering parameters in Ref. [14] shows the expected recombination loss coefficient in the magnetic field and temperature range of our interest [25], see Fig. S3.

The calculation shows signatures of three Efimov resonances at various temperatures, and confirms the suppression of the resonance features at higher temperatures. Small shifts of the resonance positions due to finite temperature effects are also visible. Based on a Gaussian plus linear fit to the calculation, we find that the resonance position shifts in the range of 100∼1000 nK are no more than +0.3%, -8% and -3% for the first, second and third resonances, respectively. The small shifts are consistent with our observation. Finally, the resonance positions (in terms of scattering length) are in remarkably good agreement with our measurement to within 15%.